

Self-organized time crystal in driven-dissipative quantum system


Ya-Xin Xiang¹, Qun-Li Lei^{1,3}, Zhengyang Bai^{2,*} and Yu-Qiang Ma^{1,3,†}

¹National Laboratory of Solid State Microstructures and School of Physics,

Collaborative Innovation Center of Advanced Microstructures, Nanjing University, Nanjing 210093, China

²State Key Laboratory of Precision Spectroscopy, East China Normal University, Shanghai 200062, China

³Hefei National Laboratory, Hefei 230088, China

 (Received 21 November 2023; revised 10 April 2024; accepted 8 July 2024; published 19 August 2024)

Continuous time crystals (CTCs) are characterized by sustained oscillations that break the time-translation symmetry. Since the ruling out of equilibrium CTCs by no-go theorems, the emergence of such dynamical phases has been observed in various driven-dissipative quantum platforms. The current understanding of CTCs is mainly based on mean-field theories, which fail to address the problem of whether the continuous time-translation symmetry can be broken in noisy, spatially extended systems absent in all-to-all couplings. Here, we propose a CTC realized in a quantum contact model through self-organized bistability. The CTCs stem from the interplay between collective dissipation induced by the first-order absorbing phase transitions and slow constant driving provided by an incoherent pump. The stability of such oscillatory phases in finite dimensions under the action of intrinsic quantum fluctuations is scrutinized by the functional renormalization group method and numerical simulations. Occurring at the edge of many-body synchronization, the CTC phase exhibits an inherent period and amplitude with a coherence time linearly diverging with system size, thus also constituting a boundary time crystal. Our results serve as a solid route towards self-protected CTCs in strongly interacting open systems.

DOI: [10.1103/PhysRevResearch.6.033185](https://doi.org/10.1103/PhysRevResearch.6.033185)

I. INTRODUCTION

Time crystals are self-organized spatiotemporal structures, first envisaged by Wilczek [1,2], that spontaneously break the time-translation symmetry imposed by underlying Hamiltonians. Since the advent of the no-go theorems stating that it is impossible to observe a spontaneously oscillating ground state (in thermal equilibrium) [3,4], there have been several efforts concentrating on time crystals in closed Floquet systems [5–10]. Alternatively, coupling to an environment leads to the dissipative version of time crystals that break the discrete/continuous time-translation symmetry of the dynamical generators [11–20].

By building up a limit cycle (LC), the rise of synchronization in diverse physical platforms, such as optomechanical oscillators [21], Rydberg gases [22–24], and hybrid atom-cavity systems [25,26], has been observed and related to the formation of continuous time crystals (CTCs). In open systems, the dissipation often associates with the quantum Langevin noise and it is probable that the fluctuations would affect the robustness of CTCs, thereby destroying the crystalline order. Notwithstanding the rapid advances in experimental studies, to what extent the CTCs remain intact

under the action of intrinsic noise is an open question worthy of theoretical endeavors.

Analogous to the famous notion of self-organized criticality (SOC), which is related to self-organization to the critical point of a continuous absorbing phase transition (APT) [27–34], the mechanism for self-organized bistability (SOB) consists in a separation of the timescale of the dynamics of the order parameter from that of the corresponding control parameter. It triggers a LC phase of the hysteresis loop of a first-order APT [34,35]. In light of the common features shared by LCs and CTCs, a new class of CTCs induced by SOB can be envisioned.

In this work, we theoretically investigate the formation and stability of CTCs beyond the mean-field (MF) approximation. Concretely, we consider a dissipative variant of the contact model characterized by the quantum and classical contact interactions between quantum emitters [36]. In the classical regime, the system undergoes continuous APTs. However, the transitions become discontinuous in the quantum regime. Upon addition of a slow loading mechanism, a nonstationary phase arises from the SOB, where the number of quantum emitters changes periodically [numerical results for three-dimensional systems sketched in Figs. 1(c) and 1(d)]. Meanwhile, the system undergoes repeated phase transitions and self-organizes to a CTC phase. Avalanches of activation, like fires spreading in a forest, trigger collective jumps from the absorbing to the active states, and terminate upon the exhaustion of emitters (trees), which in turn bring the system back into the absorbing state of slow recovery, waiting for the next jump. The CTC here is analogous to the breathing mode of a “forest-fires” model [37]. Through theoretical analysis and numerical simulations, we find that the CTCs are unstable in low-dimensional systems due to the reduced

*Contact author: zhybai@lps.ecnu.edu.cn

†Contact author: myqiang@nju.edu.cn

Published by the American Physical Society under the terms of the [Creative Commons Attribution 4.0 International](https://creativecommons.org/licenses/by/4.0/) license. Further distribution of this work must maintain attribution to the author(s) and the published article's title, journal citation, and DOI.

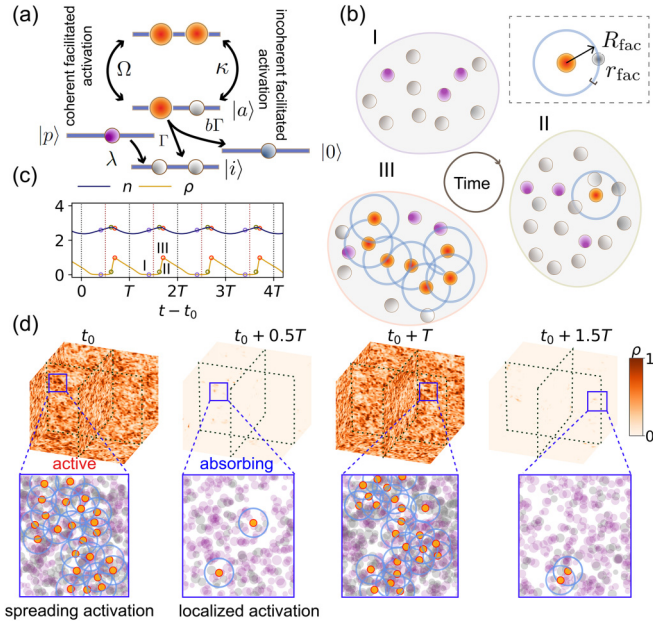


FIG. 1. (a) The effective four-level scheme. The quantum emitter in inactive state $|i\rangle$ (gray sphere) in proximity to emitters in active state $|a\rangle$ (red sphere) can become active via (in)coherent facilitated activation, and active emitters can spontaneously decay into either inactive or removed states $|0\rangle$ (blue sphere). Emitters in $|p\rangle$ state (purple sphere) are incoherently pumped to inactive state $|i\rangle$. (b) Sketch of CTC, where the contact activation occurs on the facilitation shell with a radius of R_{fac} and thickness of r_{fac} of active emitters (inset). The system typically consists of subcritical (I) and supercritical (II) states of low active densities, and supercritical highly active states (III). (c) Dynamical oscillations of the average total n and active ρ densities, corresponding to three states in (b). (d) Snapshots of the active density field from simulations.

effective barrier separating the active from the absorbing states. In addition, our CTC suffers from phase noises caused by the kinetic trapping in the absorbing state. Consequently, the coherence time diverges linearly with system size, whereas the degree of synchronization decreases in larger systems.

Overview. We begin with an introduction of the dissipative quantum contact model in Sec. II. We will start with a quantum master equation and, after determining the quantum noise operators, obtain the Heisenberg-Langevin equations. We will then consider the continuum and semiclassical limit and arrive at an effective field theory. In addition, we average out fast degrees of freedom by use of path-integral techniques (Sec. III). We then consider the thermodynamic limit and discuss the discontinuous and continuous APTs and identify the parameter regime for SOB-induced CTCs (Sec. IV). In Sec. V, we will present a systematic survey of the effects of dimensionality and system sizes on the CTCs by means of the functional renormalization group approach and numerical simulations.

II. DISSIPATIVE QUANTUM CONTACT PROCESS

A. Quantum contact model

Our model can be represented as an effective four-level system [Fig. 1(a)], where quantum emitters in active state $|a\rangle$

can spontaneously decay into the inactive state $|i\rangle$ (with rate Γ), and the inactive ones can be activated only in the vicinity of active ones both incoherently and coherently (with rates κ and Ω). Additionally, the loss of emitters due to the decaying of active emitters into the removed states $|0\rangle$ (with rate $b\Gamma$) and an incoherent coupling $|p\rangle \rightarrow |i\rangle$ that mimics injecting inactive emitters (with rate λ) are included. In free space, we can restrict the contact processes to pairs of emitters that are separated by the facilitation radius R_{fac} [38], and refer to the effective nearest neighbors (nn) of an active emitter as emitters at the border of its facilitation sphere, as illustrated in the inset of Fig. 1(b).

It follows that more precisely, a pair of nn's are those emitters whose relative distance lies within the range $[R_{\text{fac}} - r_{\text{fac}}, R_{\text{fac}} + r_{\text{fac}}]$ with a radius of R_{fac} and thickness of r_{fac} [38]. To count the number of nn's in free space, where we introduce for later convenience the function $f(a; R, r) \equiv \theta(a - R + r) - \theta(a - R - r)$, with $\theta(x)$ being the Heaviside step function, one can write

$$\hat{C}_l = \sum_k \hat{\sigma}_k^{aa} f(|\mathbf{r}_{lk}|; R_{\text{fac}}, r_{\text{fac}}), \quad (1a)$$

$$\hat{N}_l = \sum_k \hat{n}_k f(|\mathbf{r}_{lk}|; R_{\text{fac}}, r_{\text{fac}}), \quad (1b)$$

$$\hat{P}_l = \sum_k \hat{\sigma}_k^x f(|\mathbf{r}_{lk}|; R_{\text{fac}}, r_{\text{fac}}), \quad (1c)$$

where $\hat{n}_k \equiv \hat{\sigma}_k^{aa} + \hat{\sigma}_k^{ii}$ with $\hat{\sigma}_l^{\alpha\beta} \equiv |\alpha\rangle\langle\beta|$ ($\alpha, \beta = a, i, p, 0$), where l, k are indices for each emitter, and \mathbf{r}_{lk} is the relative distance between the k th and l th emitters. The operator $\hat{\sigma}_l^x = \hat{\sigma}_l^- + \hat{\sigma}_l^+$ flips the quantum state with the ladder operators $\hat{\sigma}_l^+ \equiv \hat{\sigma}_l^{ai}$ and $\hat{\sigma}_l^- \equiv \hat{\sigma}_l^{ia}$.

Under the Markovian noise, the effective dynamics of this system permits a microscopic description for the density operator $\hat{\rho}$ via a Lindblad master equation, $\partial_t \hat{\rho} = -i[\hat{H}, \hat{\rho}] + \sum_\alpha \mathcal{L}_\alpha \hat{\rho}$. The coherent activation is described by the effective Hamiltonian ($\hbar \equiv 1$ henceforth),

$$\hat{H} = \Omega \sum_l \hat{C}_l \hat{\sigma}_l^x. \quad (2)$$

The dissipative dynamics is described by the Lindblad terms $\mathcal{L}_\alpha \hat{\rho} = \sum_l [\hat{L}_{\alpha,l} \hat{\rho} \hat{L}_{\alpha,l}^\dagger - \frac{1}{2} \{ \hat{L}_{\alpha,l}^\dagger \hat{L}_{\alpha,l}, \hat{\rho} \}]$. The spontaneous inactivation of the active states is described by $\hat{L}_{d,l} = \sqrt{\Gamma} \hat{\sigma}_l^-$, and $\hat{L}_{p,l} = \sqrt{\gamma_{de}} \hat{\sigma}_l^{aa}$ represents dephasing of quantum coherence with rate γ_{de} . Meanwhile, the loss and reloading of inactive emitters are accounted for by $\hat{L}_{e,l} = \sqrt{b\Gamma} \hat{\sigma}_l^{0a}$ and $\hat{L}_{a,l} = \sqrt{\lambda} \hat{\sigma}_l^{ip}$, respectively. The incoherent contact processes are also included in Lindbladian, where the respective jump operators for the activation and inactivation of emitters are given by $\hat{L}_{b,l} = \sqrt{\kappa} \hat{C}_l \hat{\sigma}_l^+$ and $\hat{L}_{c,l} = \sqrt{\kappa} \hat{C}_l \hat{\sigma}_l^-$.

B. Heisenberg-Langevin equation

The Heisenberg-Langevin equations of motion for the operators $\hat{\sigma}_l^{x/aa}$, $\hat{\sigma}_l^y = i\hat{\sigma}_l^- - i\hat{\sigma}_l^+$, and $\hat{n}_l = \hat{\sigma}_l^{aa} + \hat{\sigma}_l^{ii}$ read

$$\partial_t \hat{\sigma}_l^{aa} = -\Gamma \hat{\sigma}_l^{aa} + \Omega \hat{C}_l \hat{\sigma}_l^y + \kappa \hat{C}_l (\hat{n}_l - 2\hat{\sigma}_l^{aa}) + \hat{\xi}_l^{aa}, \quad (3a)$$

$$\partial_t \hat{\sigma}_l^x = -\frac{\kappa \hat{N}_l + \gamma}{2} \hat{\sigma}_l^x - \kappa \hat{C}_l \hat{\sigma}_l^x - \Omega \hat{P}_l \hat{\sigma}_l^y + \hat{\xi}_l^x, \quad (3b)$$

$$\begin{aligned} \partial_t \hat{\sigma}_l^y &= -\frac{\kappa \hat{N}_l + \gamma}{2} \hat{\sigma}_l^y - \kappa \hat{C}_l \hat{\sigma}_l^y + \Omega \hat{P}_l \hat{\sigma}_l^x \\ &\quad + 2\Omega \hat{C}_l (\hat{n}_l - 2\hat{\sigma}_l^{aa}) + \hat{\xi}_l^y, \end{aligned} \quad (3c)$$

$$\partial_t \hat{n}_l = -b\Gamma \hat{\sigma}_l^{aa} + \lambda \hat{\sigma}_l^{pp} + \hat{\xi}_l^n, \quad (3d)$$

where $\gamma = \Gamma + \gamma_{de}$. Thereafter, we set the time unit to $\Gamma^{-1} = 1$. The Langevin noise operators $\hat{\xi}_l^{x/y/aa/n}$ appear because the dissipation is attributed to the coupling between the system and a large reservoir [39,40]. The quantum noise operators in accord with the jump operators then can be fixed via solving the Heisenberg equations under the above Hamiltonians in the Born-Markov approximation. Using a vectorial representation $\hat{\xi}(\mathbf{r}, t) = (\hat{\xi}_l^x(\mathbf{r}, t), \hat{\xi}_l^y(\mathbf{r}, t), \hat{\xi}_l^{aa}(\mathbf{r}, t))$, one can put the the noise correlations' covariance in a matrix form $\langle \hat{\xi}(\mathbf{r}, t) \hat{\xi}(\mathbf{r}', t') \rangle = \delta(\mathbf{r} - \mathbf{r}') \delta(t - t') \hat{M}$, with \hat{M} of the following form:

$$\begin{pmatrix} \kappa(\hat{C}\hat{n} + \hat{N}\hat{\sigma}^{aa}) + \hat{n} & -i\hat{n} & \hat{\sigma}^- - i\frac{\kappa}{2}\hat{C}\hat{\sigma}^y \\ i\hat{n} & \kappa(\hat{C}\hat{n} + \hat{N}\hat{\sigma}^{aa}) + \hat{n} & i\hat{\sigma}^- + i\frac{\kappa}{2}\hat{C}\hat{\sigma}^x \\ \hat{\sigma}^+ + i\frac{\kappa}{2}\hat{C}\hat{\sigma}^y & -i\hat{\sigma}^+ - i\frac{\kappa}{2}\hat{C}\hat{\sigma}^x & \frac{\kappa}{2}\hat{C}\hat{n} + \hat{\sigma}^{aa} \end{pmatrix}. \quad (4)$$

We refer the readers to Appendix A for the detailed derivation.

III. CLASSICAL PATH INTEGRAL FOR DENSITY FIELD

A. Coarse-grained Langevin equation

In the following, we consider the continuum limit and perform coarse graining according to

$$\rho(\mathbf{r}, t) = \mathcal{V}_{\text{fac}}^{-1} \sum_l \theta(R_{\text{fac}} - |\mathbf{r}_l - \mathbf{r}|) \text{Tr}\{\hat{\sigma}_l^{rr} \hat{\rho}\}, \quad (5a)$$

$$n(\mathbf{r}, t) = \mathcal{V}_{\text{fac}}^{-1} \sum_l \theta(R_{\text{fac}} - |\mathbf{r}_l - \mathbf{r}|) \text{Tr}\{\hat{n}_l \hat{\rho}\}, \quad (5b)$$

$$\sigma^x(\mathbf{r}, t) = \mathcal{V}_{\text{fac}}^{-1} \sum_l \theta(R_{\text{fac}} - |\mathbf{r}_l - \mathbf{r}|) \text{Tr}\{\hat{\sigma}_l^x \hat{\rho}\}, \quad (5c)$$

$$\sigma^y(\mathbf{r}, t) = \mathcal{V}_{\text{fac}}^{-1} \sum_l \theta(R_{\text{fac}} - |\mathbf{r}_l - \mathbf{r}|) \text{Tr}\{\hat{\sigma}_l^y \hat{\rho}\}, \quad (5d)$$

where $\mathcal{V}_{\text{fac}} = 4\pi R_{\text{fac}}^3/3$ is the volume of the facilitation sphere. In the long-wavelength regime, we adopt the substitution $\sum_{\text{nn}} O_{l,\text{nn}} \rightarrow \mathcal{V}_{\text{shell}} (1 + \frac{R_{\text{fac}}^2}{2} \nabla^2) O_l$ with the volume of the facilitation shell $\mathcal{V}_{\text{shell}} = 8\pi R_{\text{fac}}^2 r_{\text{fac}}$. We redefine the rates κ, Ω as $\kappa \rightarrow \kappa \mathcal{V}_{\text{shell}}, \Omega \rightarrow \Omega \mathcal{V}_{\text{shell}}$.

We further omit the operator moments generated by the two-body interactions, and arrive at a set of Langevin equations for stochastic fields $\rho, n, \sigma^x, \sigma^y$:

$$\begin{aligned} \partial_t \rho &= -\rho + \Omega \sigma^y (1 + D_\rho \nabla^2) \rho \\ &\quad + \kappa (n - 2\rho) (1 + D_\rho \nabla^2) \rho + \xi^\rho, \end{aligned} \quad (6a)$$

$$\begin{aligned} \partial_t \sigma^x &= -\frac{\sigma^x}{2} \kappa (1 + D_\rho \nabla^2) n - \kappa \sigma^x (1 + D_\rho \nabla^2) \rho \\ &\quad - \frac{\gamma}{2} \sigma^x - \Omega \sigma^y (1 + D_\rho \nabla^2) \sigma^x + \xi^x, \end{aligned} \quad (6b)$$

$$\begin{aligned} \partial_t \sigma^y &= -\frac{\sigma^y}{2} \kappa (1 + D_\rho \nabla^2) n - \kappa \sigma^y (1 + D_\rho \nabla^2) \rho \\ &\quad - \frac{\gamma}{2} \sigma^y + \Omega \sigma^x (1 + D_\rho \nabla^2) \sigma^x \rho \\ &\quad + 2\Omega (n - 2\rho) (1 + D_\rho \nabla^2) \rho + \xi^y, \end{aligned} \quad (6c)$$

$$\partial_t n = D_T \nabla^2 n - b\rho + \xi^n. \quad (6d)$$

Here the diffusion coefficient $D_\rho = \kappa R_{\text{fac}}^2/2 + D_T$ and D_T is the thermal diffusion coefficient of atoms. The classical noise covariance M_{lm} is constructed from the Hermitian parts of the quantum noise covariance (4), i.e., $M_{lm} = \langle \hat{M}_{ml} + \hat{M}_{lm} \rangle / 2$, where $l, m \in \{x, y, \rho\}$ [36,41]. Since the noise sources are Markovian, we drop the contributions of the spatial gradients to the noise covariance; then the covariance matrix \mathbf{M} reads

$$\mathbf{M} = \begin{pmatrix} (1 + 2\kappa\rho)n & 0 & \frac{\sigma^x}{2} \\ 0 & (1 + 2\kappa\rho)n & \frac{\sigma^y}{2} \\ \frac{\sigma^x}{2} & \frac{\sigma^y}{2} & (\kappa n + 1)\rho \end{pmatrix}. \quad (7)$$

With respect to the total density field n , there is

$$\langle \xi^n(\mathbf{r}, t) \xi^n(\mathbf{r}', t') \rangle = b\rho(\mathbf{r}, t) \delta(\mathbf{r} - \mathbf{r}') \delta(t - t'). \quad (8)$$

Given that the number of emitters in the p state is large enough to be regarded constant throughout the dynamics of other density fields, contribution of the loading process to (8) is ignored.

B. Dynamic path integral

From the Langevin equations (6a)–(6c), one can construct a functional integration representation in terms of the Janssen–de Dominicis formalism [42], upon introducing an auxiliary Martin-Siggia-Rose response field [43].

The dynamics of the fields $\sigma^{x/y}$ described by Eqs. (6b) and (6c) relaxes over the timescale of $(\kappa n + \gamma)^{-1}$, which is typically shorter than those of the two density fields. Treating $\sigma^{x/y}$ as uniform fields and the slow variables ρ, n as external parameters, a conditional transitional probability corresponding to Eqs. (6b) and (6c) in Itô's discretization can be written following Refs. [44,45]. The resulting transition probability can be recast into a Gaussian integral; upon introducing the imaginary, response fields $\tilde{\sigma}^x, \tilde{\sigma}^y$ conjugate to σ^x, σ^y (called the Martin-Siggia-Rose auxiliary fields and related to the dynamic responses of σ^x, σ^y to perturbations), respectively, one obtains

$$\begin{aligned} P(\sigma_{j+1}^x, \sigma_{j+1}^y | \sigma_j^x, \sigma_j^y) &= \prod_{l=x,y} \int_{-i\infty}^{i\infty} \frac{d\tilde{\sigma}_{j+1}^l}{2\pi i} \exp \left[-\tilde{\sigma}_{j+1}^l (\sigma_{j+1}^l - \sigma_j^l - dt \mathcal{F}_{\sigma^l, j}) \right. \\ &\quad \left. + \frac{1}{2} dt M_{ll, j} (\tilde{\sigma}_{j+1}^l)^2 \right], \end{aligned} \quad (9)$$

where the subscripts j and $j+1$ indicate the discrete time steps, $dt = t_{j+1} - t_j$ is the time step, $M_{ll, j} = \text{Var}(\xi_j^l)$ is the noise covariance, and $\mathcal{F}_{\sigma^l, j}$ is the deterministic part of the Langevin equations (6b) and (6c).

The transition probability during a finite time follows from the summation of all trajectories with fixed initial and

ending points, which can be omitted for nonequilibrium steady states [45]. By summing up all spatiotemporal configurations instead of trajectories, we obtain a path integral in the $dt \rightarrow 0$ limit,

$$\mathcal{Z} = \int \mathcal{D}[\sigma^x, \tilde{\sigma}^x, \sigma^y, \tilde{\sigma}^y] \mathcal{J} e^{-S_\sigma}, \quad (10)$$

in which the action $S_\sigma = \int \sum_{l=x,y} \tilde{\sigma}^l (\mathcal{F}_{\sigma^l} - \frac{M_l}{2} \tilde{\sigma}^l)$ and the Jacobian $\mathcal{J} = 1$ upon a precise ordering of times such that all the response fields appear at a time larger than or equal to the times of their conjugate fields [45,46] (i.e., in Itô's discretization). Since the density fields ρ, n serve as external parameters, we have excluded contributions of $M_{\rho x}, M_{\rho y}$ and introduced the shorthand notation $\int = \int dt dr$.

Likewise, we introduce a response field $\tilde{\rho}$ to rewrite the Langevin equation (6a) into a path integral. The resultant action functional consists of a bare, $\sigma^{x/y}$ -independent part S_ρ ,

$$S_\rho = \int \tilde{\rho} \left[(\partial_t - D_\rho \nabla^2) \rho + \rho - \kappa(n - 2\rho)\rho - \frac{1 + \kappa n}{2} \rho \right], \quad (11)$$

and a part $S_{\rho,\sigma}$ arising from the coupling between the slow and fast variables,

$$S_{\rho,\sigma} = - \int \Omega \tilde{\rho} \rho \sigma^y. \quad (12)$$

The total action functional related to the coherence fields σ^x, σ^y is the sum $S_\sigma + S_{\rho,\sigma}$. We then perturbatively integrate out σ^x, σ^y to arrive at an effective action for the active density field (see Appendix B for details),

$$S[\rho, \tilde{\rho}] = \int \tilde{\rho} \left[(\partial_t - D_\rho \nabla^2 + u_2) \rho + u_3 \rho^2 + u_4 \rho^3 - \frac{\mu}{2} \tilde{\rho} \right], \quad (13)$$

where $u_2 = 1 - n\kappa - 256n^2\Omega^4/(n\kappa + \gamma)^7$, $u_3 = 2[\kappa - 2n\Omega^2/(n\kappa + \gamma)]$, $u_4 = 8\Omega^2/(n\kappa + \gamma)$, and $\mu = (1 + n\kappa)\rho + 4n\Omega^2\rho^2/(n\kappa + \gamma)^2$ are the coupling constants.

IV. DISSIPATIVE PHASE TRANSITION

Mean-field analysis

With the total density n conserved ($b, \lambda = 0$), the static phases are determined by the solutions to the saddle-point equations following variation of action (13) with $\tilde{\rho}, \tilde{n} = 0, D_T \rightarrow \infty$. The corresponding phase boundaries are shown in Fig. 2(a). In the classical regime, the bistable region within the two boundaries vanishes, and in accord, as shown in Fig. 2(b) the active density increases continuously with the incoherent activation rate κ . The limiting case $\Omega = 0, \kappa \neq 0$ has been related to SOC in driven-dissipative Rydberg gases [37,38,47], whereas in the quantum regime, the bistable region within the two boundaries indicates that the systems undergo discontinuous APTs when the total density n exceeds a critical value [see Figs. 2(c) and 2(d)], which is an element of SOB-induced CTCs to be discussed later.

Having identified the regime for first-order APTs, sustained oscillations can arise from the interplay between loss and reloading of emitters ($b, \lambda \neq 0$). Our proposal for

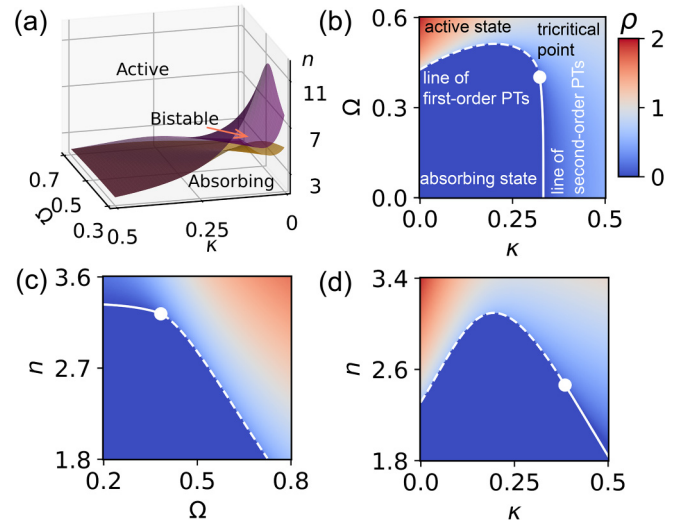


FIG. 2. Phase diagrams with conserved total density ($b, \lambda = 0$) for (b) $n = 3$, (c) $\kappa = 0.3$, and (d) $\Omega = 0.5$. The system can undergo a phase transition from a phase with zero active density to an active phase with nonzero active density (dis)continuously upon crossing the (dashed) solid lines from below. The two lines terminate at a tricritical point (dots). (a) The two surfaces are the phase boundaries. Discontinuous APTs ensue when the two surfaces are separated from each other.

SOB-induced CTCs is encoded in the Langevin equations for the density fields ρ, n as follows:

$$\partial_t \rho = D_\rho \nabla^2 \rho + \tau n - u_2 \rho - u_3 \rho^2 - u_4 \rho^3 + \eta, \quad (14a)$$

$$\partial_t n = D_T \nabla^2 n - b\rho + \lambda + \xi^n, \quad (14b)$$

where η, ξ^n are Markovian white noises with vanishing mean and respective variance $\mu + \tau n$ and $b\rho$. To prevent the system from trapping in absorbing states, a small driving τn is added. Throughout the paper, we fix $\tau = 10^{-7}$, $b = 0.01$, $D_T = 1$, $n_p = 1$, $\kappa = 0$, $\Omega = 0.5$, and $\gamma = 2$, unless otherwise stated.

We proceed to determine the dynamic phases by employing the relation between the poles of the correlation functions and the dynamic criticality (instabilities at finite frequencies) [17,48–50]. We start with an extended dynamic action functional,

$$S = \int \tilde{n} \left[(\partial_t - D_T \nabla^2) n + b\rho - \lambda - \frac{b\rho}{2} \tilde{n} \right] + \int \tilde{\rho} \left[\partial_t - D_\rho \nabla^2 + u_2 + u_3 \rho + u_4 \rho^2 - (\mu_1 + \mu_2 \rho) \tilde{\rho} \right] \rho, \quad (15)$$

where $\mu_1 = (1 + n\kappa)/2$, $\mu_2 = 2n\Omega^2/(n\kappa + \gamma)^2$. Let the stationary solutions (fixed points) in a saddle-point approximation ($\tilde{n}_0, \tilde{\rho}_0 = 0$) be $\rho_{\text{fp}} = \rho_0, n_{\text{fp}} = n_0$. We expand the action (15) around the fixed points ρ_0, n_0 in terms of the small deviations from them. After performing the Fourier transform, we arrive at

$$S = \frac{1}{2} \int_{q,\omega} \begin{pmatrix} \tilde{\rho}_{-q,-\omega} \\ \rho_{-q,-\omega} \\ \tilde{n}_{-q,-\omega} \\ n_{-q,-\omega} \end{pmatrix} \mathcal{A} \begin{pmatrix} \tilde{\rho}_{-q,-\omega} \\ \rho_{-q,-\omega} \\ \tilde{n}_{-q,-\omega} \\ n_{-q,-\omega} \end{pmatrix}, \quad (16)$$

with the Hermitian coupling matrix of a homogeneous phase $A(q=0, \omega)$ given by

$$\begin{pmatrix} -2\rho_0(\mu_1 + \mu_2\rho_0) & -i\omega - J_\rho & 0 & -J_n \\ i\omega - J_\rho & 0 & b & 0 \\ 0 & b & -b\rho_0 & -i\omega \\ -J_n & 0 & i\omega & 0 \end{pmatrix}, \quad (17)$$

where $J_x = -\partial_x(u_2\rho + u_3\rho^2 + u_4\rho^3)_{\rho_0, n_0}$, $x = n, \rho$. The density-density correlation functions within the Gaussian approximation are the inverse of the harmonic coupling matrix $\mathbf{G} = \mathbf{A}^{-1}$, namely,

$$\langle \rho_\omega \rho_{-\omega} \rangle = \frac{-\rho_0 [bJ_n^2 + 2\omega^2(\mu_1 + \mu_2\rho_0)]}{\omega^2(J_\rho^2 + \omega^2) - 2bJ_n\omega^2 + b^2J_n^2}. \quad (18)$$

The unequal retarded time correlation is controlled by the poles of Eq. (18),

$$\omega = i\frac{J_\rho}{2} \pm \sqrt{bJ_n - \frac{J_\rho^2}{4}}, \quad (19)$$

of which the real parts are the energies of collective modes, while the imaginary parts represent the relaxation rates of these modes and must be negative; otherwise, the correlation will diverge over time.

When $J_\rho \approx 0$, a pair of poles with energies $\varepsilon_\pm = \pm\sqrt{bJ_n}$ touches the real axis whereupon the correlation function diverges like $|J_\rho|^{-1}$ at a finite frequency ε_+ , signaling the breaking of time-translation invariance. Such an instability in the frequency domain is related to a dynamic criticality, and hence the dynamic critical point $\lambda_c = \arg_\lambda J_\rho = 0$, which separates the stable and unstable fixed points n_{FP} and ρ_{FP} as displayed in Fig. 3(a). Also, in the presence of first-order APTs, we can determine how the critical loading rate λ_c varies with the classical and quantum contact activation rates κ, Ω , which is shown in Fig. 3(b).

A lack of time-translation symmetry should suffice to indicate an oscillatory phase. As a demonstration, we numerically integrate Eqs. (14a) and (14b) in the noiseless limit for $\lambda < \lambda_c$. The CTCs feature alternating sharp switching (jumps) between the states with low and high active densities [Fig. 3(d), upper panel] with a period $\propto \lambda^{-1}$ [Fig. 3(d), lower panel]. The rather large timescale compared with the lifetime of an individual emitter ($\lambda^{-1} \gg 1$) suggests that the jumps herein are essentially classical and collective, reminiscent of the jumpy transitions between distinct collective phases reported in Refs. [51–53].

V. STABILITY OF SELF-ORGANIZED OSCILLATION IN FINITE SYSTEMS

The remaining part is devoted to a systematic study of the CTC in finite systems.

A. Renormalization group approach

We first discuss how dimensionality affects the stability of the CTCs. In lower dimensions, the effective barrier between the two states can be reduced. The jumps might occur at a wider range of total densities, thus destroying the long-range time crystalline order. To acquire a quantitative description,

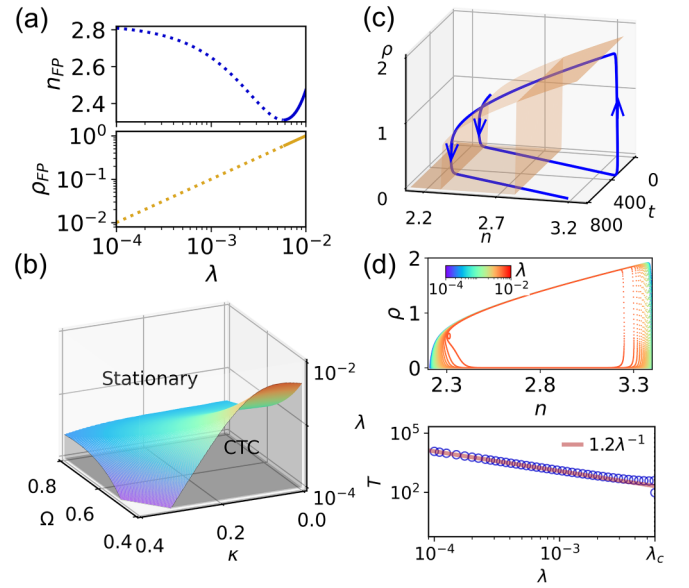


FIG. 3. Phase diagrams for SOB. (a) Stable (solid lines) and unstable (dashed lines) fixed points. (b) The surface represents the critical rate λ_c (color coded) that separates a stationary phase from a CTC phase, corresponding to stable and unstable fixed points. (c) The CTC phase that consists of self-organized jumps (blue arrows) between the active and the absorbing phases (orange surfaces) for $\lambda = 3.2 \times 10^{-3}$. (d) Phase-space trajectories (upper) and periods (lower) as a function of λ .

we adopt a functional renormalization group (fRG) approach via the Wetterich equation [45,54,55],

$$\partial_k \Gamma_k = \frac{1}{2} \text{Tr}[(\Gamma_k^{(2)} + R_k)^{-1} \partial_k R_k], \quad (20)$$

where Γ_k is the nonequilibrium equivalent of the Gibbs free energy in the presence of a masslike regulator R_k that decouples short-wavelength modes from long-wavelength ones. By suppressing the low-energy fluctuations, the regulated action Γ_k interpolates smoothly between the microscopic action Γ_0 and the original MF one, $\Gamma_\Lambda = \mathcal{S}$, as the infrared cutoff k varies within the range $k \in [0, \Lambda]$. Rather than evaluating the exact equation (20) directly, which is numerically demanding, we resort to the well-established local potential approximation (LPA) ansatz [55], according to which the interaction part of the action Γ_k corresponds to an effective potential evaluated with uniform background field. This allows us to obtain the flows of the phase structure with decreasing cutoff momentum k for various values of n in different dimensions. Details of this procedure are presented in Appendix C.

The resulting effective potential $\Phi_f(\rho)$ and the corresponding phase diagram are shown in Fig. 4. In $d=1$, as n increases, the position of the local minimum shifts continuously from the origin to a finite value, indicating a continuous transition [Fig. 4(a)]. In $d \geq 2$, however, increasing n induces the appearance of a second local minimum at the finite density, apart from the local minimum at the origin, with a barrier in between, indicating a first-order transition [Figs. 4(b) and 4(c)]. In addition, the barrier is higher in $d=3$ than $d=2$, suggesting a weaker first-order transition in lower dimensions. The phase diagram in accord is shown in Fig. 4(d), where

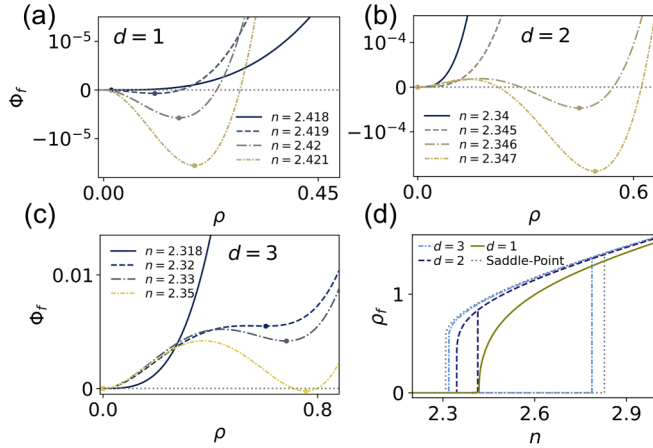


FIG. 4. The effective potential Φ_f as a function of the active density field ρ for different n in (a) $d = 1$, (b) $d = 2$, (c) $d = 3$. The active/absorbing phases are determined by the local minima (dots). (d) The corresponding phase diagram in comparison with that obtained via saddle-point approximation.

we can infer that discontinuous transitions are expected for $d \geq 2$. Compared with the MF results, the coexistence region becomes narrower for a lower dimensionality. The fRG results indicate that CTCs are possible in $d \geq 2$. The three-dimensional CTC is protected by a higher barrier and is thus more stable.

B. Numerical simulations

We then numerically simulate Eqs. (14a) and (14b), deploying the operator-splitting scheme [56,57], and record the time series of the average active and total densities. As a measure of time crystallinity, we computed the two-time correlation functions $G_x(\Delta t) \equiv \langle x(t) \rangle_t^{-2} \langle x(t)x(t + \Delta t) \rangle_t$, for $x = n, \rho$ [23], and manifest constant periodic oscillations for perfect time crystals [23]. Correspondingly, their Fourier spectra $G_x(\omega)$ peak at the integer multiples of their respective inherent frequencies ω_m .

The simulation results for $d = 1, 2$ are shown in Fig. 5. Within the parameter regime for CTC, the time series show no sign of periodic oscillations in one-dimensional systems [Fig. 5(a)]. This is consistent with the absence of the first-order APTs therein. In contrast, in two dimensions, the average densities oscillate over time [Fig. 5(b)], albeit at a smaller scale compared with their three-dimensional counterparts [Fig. 6(a)], in accordance with a weaker first-order APT for $d = 2$ revealed by the fRG analysis. Furthermore, the associated two-time correlation function $G_\rho(\Delta t)$ remains periodic for a finite time, with its Fourier spectra $G_\rho(\omega)$ peaking at the inherent frequency ω_m [see Figs. 5(c) and 5(d), respectively]. These results suggest the rise of the CTC phase for $d \geq 2$. Given the enhanced stability of CTCs in higher dimensionalities, in what follows, we restrict our discussion to $d = 3$.

As evinced in Fig. 6(a), the time series of the average densities become progressively regular as we increase the edge length L of the system. Meanwhile, we can infer from Fig. 6(b) that in enlarged systems, the amplitude of $G_n(\Delta t)$

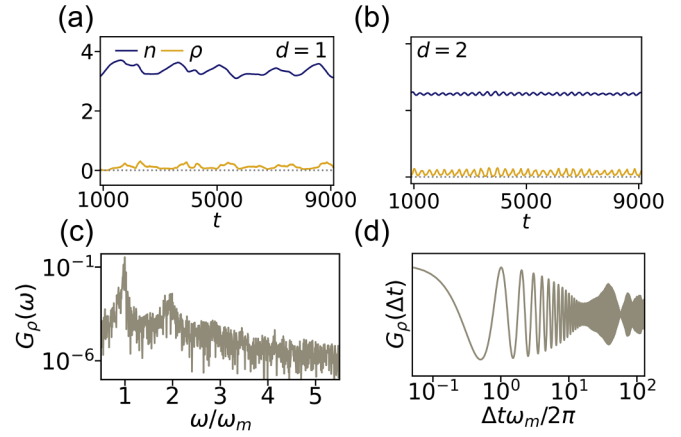


FIG. 5. Time series of the total and active densities from simulations in (a) one dimensions with edge length $L = 10^4$ and (b) two dimensions with edge length $L = 256$. (c), (d) The two-time correlation function and its Fourier spectra of (b), respectively. Parameters are $\lambda = 1.2 \times 10^{-3}$.

varies more slowly, and the Fourier spectra are more sharply peaked at $\omega/\omega_m = 1, 2, 3, \dots$, both suggestive of the emergence of more periodic structures in time. In addition, once the time crystalline order is built, the period $T \equiv 2\pi/\omega_m$ remains invariant with diverging L [Fig. 7(a)] and is thus inherent to CTCs. The existence of sustained oscillations with an intrinsic amplitude and frequency suggests that our CTCs are also a realization of boundary time crystals (BTCs) [15].

Stimulated and spontaneous sharp transitions between multiple (meta)stable states in quantum and classical systems are referred to as (collective) jumps [51–53,58]. The SOB-induced CTCs thus also entail a succession of collective jumps where the time series experience abrupt changes. We call the jumps from the absorbing (active) and the active (absorbing) states as upward (downward), and denote them with red (blue)

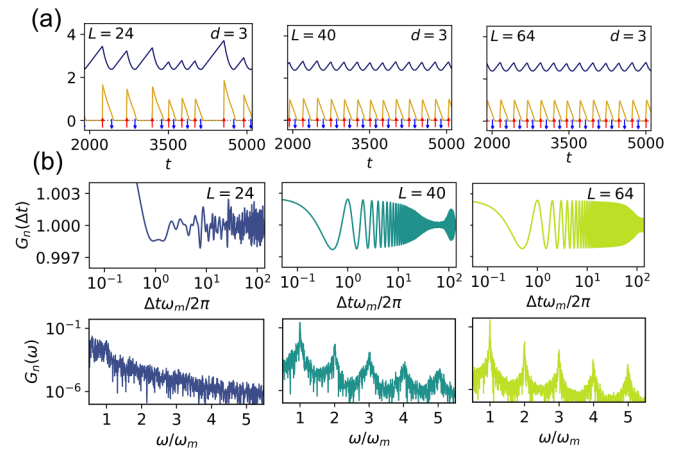


FIG. 6. (a) Time series of the densities with collective jumps marked by red (blue) arrows in three-dimensional systems for $L = 24$ (left), $L = 40$ (middle), and $L = 64$ (right). (b) The autocorrelation functions $G_n(\Delta t)$ (upper) and their Fourier spectra $G_n(\omega)$ (lower), where the first peak ω_m dictates (e) the period $T = 2\pi/\omega_m$. We select $\lambda = 3.2 \times 10^{-3}$ for (a) and (b).

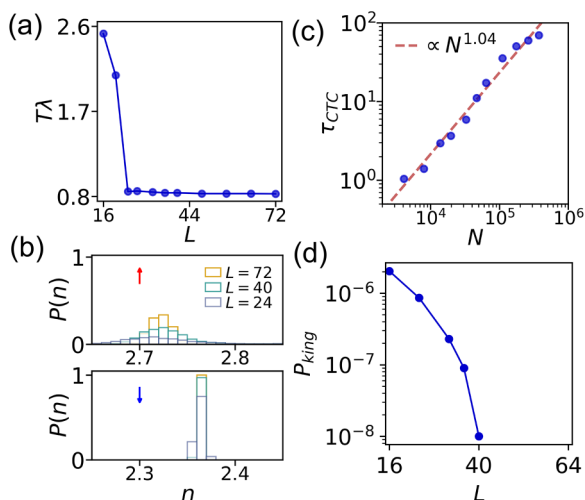


FIG. 7. (a) Rescaled period obtained from the inverse of the location of the highest peak of the Fourier spectra. (b) Probability distribution of the average total densities at which upward (upper) and downward (lower) jumps occur for varying L . (c) The coherence time τ_{CTC} defined as the ratio of the period to its standard deviation, where $N = L^3$ is the system volume. (d) The occurrence probability of king avalanches. We choose $d = 3$, $\lambda = 3.2 \times 10^{-3}$ for (a)–(d).

arrows. Exemplary time series with detected jumps are shown in Fig. 6(a), whence it is evinced that more regular jumps occur in larger systems. As a measure of time crystalline order encoded in jumps, we construct the distribution $P(n)$ of the average total density at which these jumps occur, and we find that it converges as the system is enlarged [Fig. 7(b)].

Since upward jumps always lead to correlations among distant emitters (avalanches), the enhanced time crystallinity cannot be explained through the method of system-size expansion [14,59–61]. The irregularity in the time series features a significant increase in the total density, followed by an abrupt decrease in the active and total densities [see Fig. 6(a), left panel]. For low loading rates, such events have been attributed to the system falling into the absorbing state, and the consequent overloading in turn brings about system-spanning activation avalanches [62,63]. For a three-dimensional CTC with a volume of $N = L^3$, the accumulated phase shift $\Delta\theta$ per cycle is approximately the probability of kinetic trapping in the absorbing phase, $\sim 1/(TN\tau)$, and CTC should remain coherent over the timescale (rescaled by T) $\tau_{CTC} \approx 2\pi T/\Delta\theta$. We then estimate the coherence time from simulations by extracting the phase shifts via $\Delta\theta = 2\pi\langle\Delta T\rangle/T$, where $\langle\Delta T\rangle$ is the standard deviation of the period. The results are plotted in Fig. 7(c), where the coherence time increases nearly linearly with the volume with a prefactor of $1.5(4) \times 10^{-4}$. It is easy to reconcile the finite correlations and diverging coherence time in the $N \rightarrow \infty$ limit because the absorbing state is devoid of fluctuations and has a lifetime inversely proportional to N .

Also, the next upward jump following the kinetic trapping is likely to trigger huge avalanches. To test this idea, we count space-time activation avalanches by connecting sites with active densities larger than a threshold (τ) as neighbors in the time-forward direction and grouping them into clusters. The occurrence probability of huge avalanches (king avalanches,

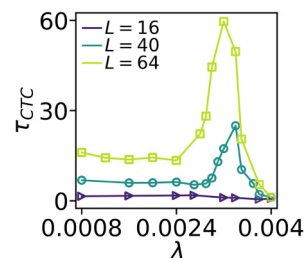


FIG. 8. The coherence time as a function of system size L and loading rate λ for $d = 3$. The range of λ where CTC emerges widens with L .

defined as those containing more than half the total number of sites) decreases as the system becomes larger [Fig. 7(d)], in line with the longer coherence time [Fig. 7(c)]. A comparison of τ_{CTC} among various loading rates and system sizes is displayed in Fig. 8; the regime for CTCs indicated by the significantly increased coherence time lies between that for the aperiodic oscillations and the fluctuating uniform ones, and widens in larger systems.

Frequent huge avalanches induce coherent changes in active and total densities among a great many sites and thus reflect the underlying synchrony at its highest level. However, a lack of synchrony results in stationary states with small fluctuations that conserve time-translation invariance. Sustained periodic oscillations reside in between the above two scenarios, where discontinuous phase transitions spontaneously generate finite-range correlations, which are enough to trigger coherence among local sites and yet unable to support a global synchronization in infinite systems. In other words, SOB-induced CTCs arise at the edge of many-body synchronization.

VI. CONCLUSION

In this work, we propose a mechanism to realize self-protected CTCs with diffusive couplings. Our analysis is not restricted to APTs and can be generalized to other systems with bi-/multistability. Our CTCs can be interpreted as a BTC [15], where the reservoir plays the role analogous to the bulk Hamiltonian. The model here can be implemented with coherent laser-driven Rydberg atoms in the antiblockade regime, where the electronic ground (Rydberg) states can be mapped to the inactive (active) states [36,38,47]. The relative importance of the coherent and incoherent activation processes can be controlled by driven lasers.

Revealing how temporal organization arises from the SOB-induced bifurcation in quantum many-body systems, our study extends the dynamical phase diagram for both SOB and instability-related LCs [34,64,65]. Alongside the coherent-state path integral formalism for reaction-diffusion systems [66–68], the procedures facilitate the study of real-world critical-like events [33,62,69–72] through controllable platforms.

Finally, since our current analysis focused mainly on the semiclassical limit, developing alternative methods such as the Keldysh functional integral approach [73,74] that preserves the structure of the Lindbladian and retains more quantum signatures can be a future task.

ACKNOWLEDGMENTS

This work is supported by the National Natural Science Foundation of China under Grants No. 12347102 and No. 12274131, and Innovation Program for Quantum Science and Technology under Grant No. 2024ZD0300101. We are grateful to the High Performance Computing Center (HPCC) of Nanjing University for performing the numerical calculations in this paper on its blade cluster system. We also acknowledge the support by Jiangsu Physical Science Research Center.

APPENDIX A: QUANTUM NOISE OPERATOR

We follow [36,41] to write the three local reservoir Hamiltonian, where \hat{H}_d represents the spontaneous decay, and \hat{H}_b and \hat{H}_c account for the incoherent contact activation and the inverse process, respectively. For each emitter, the reservoir Hamiltonians are written as

$$\hat{H}_d = \sum_q \lambda_q^d (\hat{\sigma}^+ \hat{d}_q + \hat{d}_q^\dagger \hat{\sigma}^-) + \sum_q \omega_q^d \hat{d}_q^\dagger \hat{d}_q, \quad (\text{A1a})$$

$$\begin{aligned} \hat{H}_b = & \sum_{q,\text{nn}} \lambda_q^b (\hat{\sigma}_{\text{nn}}^{aa} \hat{b}_q^\dagger \hat{\sigma}^+ + \hat{\sigma}^{aa} \hat{b}_{q,\text{nn}}^\dagger \hat{\sigma}_{\text{nn}}^+ + \text{H.c.}) \\ & + \sum_q \omega_q^c \left(\hat{b}_q^\dagger \hat{b}_q + \sum_{\text{nn}} \hat{b}_{q,\text{nn}}^\dagger \hat{b}_{q,\text{nn}} \right), \end{aligned} \quad (\text{A1b})$$

$$\begin{aligned} \hat{H}_c = & \sum_{q,\text{nn}} \lambda_q^b (\hat{\sigma}_{\text{nn}}^{aa} \hat{\sigma}^+ \hat{c}_q + \hat{\sigma}^{aa} \hat{\sigma}_{\text{nn}}^+ \hat{c}_{q,\text{nn}} + \text{H.c.}) \\ & + \sum_q \omega_q^c \left(\hat{c}_q^\dagger \hat{c}_q + \sum_{\text{nn}} \hat{c}_{q,\text{nn}}^\dagger \hat{c}_{q,\text{nn}} \right), \end{aligned} \quad (\text{A1c})$$

where the operators $\hat{d}_q, \hat{b}_q, \hat{c}_q$ are bosonic bath modes with their respective frequencies $\omega_q^{d/b/c}$, and the coupling strength $\lambda_q^{d/b/c}$. In addition, to keep the noise Markovian, we discard the possible noise correlations between a pair of neighboring sites, which arises from the Hamiltonians $\hat{H}_{b/c}$ acting on the neighbors of a given site, and vice versa [41].

From now on, the indices for emitters within these Hamiltonians are dropped because the noise is Markovian, and the operators $\hat{d}_q, \hat{b}_q, \hat{c}_q$ are bosonic bath modes with their respective frequencies $\omega_q^{d/b/c}$ and the coupling strength $\lambda_q^{d/b/c}$. In addition, we discard the possible noise correlations between a pair of neighboring sites, which arises from the Hamiltonians $\hat{H}_{b/c}$ acting on the neighbors of a given site, and vice versa [41]. The noise operators in accord with the jump operators in the main text are fixed via solving the Heisenberg equations under the above Hamiltonians in the Born-Markov approximation.

1. Spontaneous decay

To begin with, let us consider the spontaneous decay (inactivation). The Heisenberg equations under the action of \hat{H}_d read

$$\partial_t \hat{\sigma}^{aa} = i[\hat{H}_d, \hat{\sigma}^{aa}] = i \sum_q \lambda_q^d (\hat{d}_q^\dagger \hat{\sigma}^- - \hat{\sigma}^+ \hat{d}_q), \quad (\text{A2a})$$

$$\partial_t \hat{\sigma}^+ = i[\hat{H}_d, \hat{\sigma}^+] = -i \sum_q \lambda_q^d \hat{d}_q^\dagger \hat{\sigma}^z, \quad (\text{A2b})$$

$$\partial_t \hat{d}_q = i[\hat{H}_d, \hat{d}_q] = -i\lambda_q^d \hat{\sigma}^- - i\omega_q^d \hat{d}_q. \quad (\text{A2c})$$

Formal integration of the last equation (A2c) leads to

$$\hat{d}_q(t) = \hat{d}_q(0) e^{-i\omega_q^d t} - i\lambda_q^d \int_0^t dt' \hat{\sigma}^-(t') e^{-i\omega_q^d(t-t')}. \quad (\text{A3})$$

Then the remaining two equations become

$$\begin{aligned} \partial_t \hat{\sigma}^{aa} = & i \sum_q \lambda_q^d [\hat{d}_q^\dagger(0) \hat{\sigma}^-(t) e^{i\omega_q^d t} - \text{H.c.}] \\ & - \sum_q (\lambda_q^d)^2 \int_0^t dt' [\hat{\sigma}^+(t') \hat{\sigma}^-(t) e^{i\omega_q^d(t-t')} + \text{H.c.}], \end{aligned} \quad (\text{A4a})$$

$$\begin{aligned} \partial_t \hat{\sigma}^+ = & -i \sum_q \lambda_q^d \hat{d}_q^\dagger(0) \hat{\sigma}^z(t) e^{i\omega_q^d t} \\ & + \sum_q (\lambda_q^d)^2 \int_0^t dt' \hat{\sigma}^+(t') \hat{\sigma}^z(t) e^{i\omega_q^d(t-t')}. \end{aligned} \quad (\text{A4b})$$

The first addends on the right hand side of Eqs. (A4a) and (A4b) are the noise operators corresponding to the spontaneous decay process,

$$\hat{\xi}_d^{aa}(t) = i \sum_q \lambda_q^d [\hat{d}_q^\dagger(0) \hat{\sigma}^-(t) e^{i\omega_q^d t} - \text{H.c.}], \quad (\text{A5a})$$

$$\hat{\xi}_d^+(t) = -i \sum_q \lambda_q^d \hat{d}_q^\dagger(0) \hat{\sigma}^z(t) e^{i\omega_q^d t}, \quad (\text{A5b})$$

and the second addends represent the dissipation.

In the Born-Markov approximation, the summation over all frequencies contributes to a delta function $\delta(t-t')$; then the dissipation rate is related to the effective coupling constant $\lambda^d(0) = \sum_q \delta(\omega_q^d) \lambda_q^d$ and the bath density of states at zero frequency, $D(0) = \sum_q \delta(\omega_q^d)$, via $2\pi D(0) [\lambda^d(0)]^2 = 1$. It follows from $\langle \cdot \rangle = \text{Tr}\{(\dots) \hat{\rho}_d^0\}$ and $\langle \hat{d}_q^\dagger \hat{d}_q \rangle = n_q = 0$, that $\langle \hat{\xi}_d^{aa/+} \rangle = 0$, and the nonvanishing covariance reads

$$\langle \hat{\xi}_d^{aa}(t) \hat{\xi}_d^{aa}(t') \rangle = \hat{\sigma}^{aa} \delta(t-t'), \quad (\text{A6a})$$

$$\langle \hat{\xi}_d^{aa}(t) \hat{\xi}_d^+(t') \rangle = \hat{\sigma}^+ \delta(t-t'), \quad (\text{A6b})$$

$$\langle \hat{\xi}_d^-(t) \hat{\xi}_d^+(t') \rangle = \hat{n} \delta(t-t'). \quad (\text{A6c})$$

Together with $\hat{\xi}_d^x = \hat{\xi}_d^+ + \hat{\xi}_d^-$, $\hat{\xi}_d^y = -i\hat{\xi}_d^+ + i\hat{\xi}_d^-$, one arrives at

$$\langle \hat{\xi}_d^{aa}(t) \hat{\xi}_d^x(t') \rangle = \hat{\sigma}^+ \delta(t-t'), \quad (\text{A7a})$$

$$\langle \hat{\xi}_d^{aa}(t) \hat{\xi}_d^y(t') \rangle = -i\hat{\sigma}^+ \delta(t-t'), \quad (\text{A7b})$$

$$\langle \hat{\xi}_d^x(t) \hat{\xi}_d^y(t') \rangle = -i\hat{n} \delta(t-t'), \quad (\text{A7c})$$

$$\langle \hat{\xi}_d^x(t) \hat{\xi}_d^x(t') \rangle = \langle \hat{\xi}_d^y(t) \hat{\xi}_d^y(t') \rangle = \hat{n} \delta(t-t'). \quad (\text{A7d})$$

2. Incoherent contact processes

Hereafter, we introduce $\lambda_q = \lambda_q^{b/c}$, $\omega_q = \omega_q^{b/c}$ since the frequencies and the coupling of the two baths are the same. In the same spirit as in Sec. A 1, the Hamiltonian \hat{H}_b yields the

following equations:

$$\partial_t \hat{\sigma}^+ = -i \sum_{q, \text{nn}} \lambda_q [\hat{\sigma}_{\text{nn}}^{aa} \hat{\sigma}^z \hat{b}_q - (\hat{\sigma}^+ \hat{\sigma}_{\text{nn}}^- \hat{b}_{q, \text{nn}} + \text{H.c.})], \quad (\text{A8a})$$

$$\partial_t \hat{\sigma}^{aa} = i \sum_{q, \text{nn}} \lambda_q (\hat{\sigma}_{\text{nn}}^{aa} \hat{\sigma}^- \hat{b}_q - \text{H.c.}), \quad (\text{A8b})$$

$$\partial_t \hat{b}_q = -i \sum_{\text{nn}} \lambda_q \hat{\sigma}_{\text{nn}}^{aa} \hat{\sigma}^+ - i\omega_q \hat{b}_q, \quad (\text{A8c})$$

$$\partial_t \hat{b}_{q, \text{nn}} = -i\lambda_q \hat{\sigma}_{\text{nn}}^{aa} \hat{\sigma}^+ - i\omega_q \hat{b}_{q, \text{nn}}. \quad (\text{A8d})$$

The equations under the Hamiltonian \hat{H}_c read

$$\partial_t \hat{\sigma}^+ = -i \sum_{q, \text{nn}} \lambda_q [\hat{\sigma}_{\text{nn}}^{aa} \hat{c}_q^\dagger \hat{\sigma}^z - (\hat{\sigma}^+ \hat{\sigma}_{\text{nn}}^+ \hat{c}_{q, \text{nn}} + \text{H.c.})], \quad (\text{A9a})$$

$$\partial_t \hat{\sigma}^{aa} = i \sum_{q, \text{nn}} \lambda_q (\hat{\sigma}_{\text{nn}}^{aa} \hat{c}_q^\dagger \hat{\sigma}^- - \text{H.c.}), \quad (\text{A9b})$$

$$\partial_t \hat{c}_q = -i \sum_{\text{nn}} \lambda_q \hat{\sigma}_{\text{nn}}^{aa} \hat{\sigma}^- - i\omega_q \hat{c}_q, \quad (\text{A9c})$$

$$\partial_t \hat{c}_{q, \text{nn}} = -i\lambda_q \hat{\sigma}_{\text{nn}}^{aa} \hat{\sigma}^- - i\omega_q \hat{c}_{q, \text{nn}}. \quad (\text{A9d})$$

Similar to the procedure in Sec. A 1, by solving Eqs. (A8) and (A9), the spin operators $\hat{\sigma}^{aa/+}$ yield the following noise operators:

$$\begin{aligned} \hat{\xi}_b^+(t) &= -i \sum_q \lambda_q \hat{C}(t) \hat{\sigma}^z(t) \hat{b}_q(0) e^{-i\omega_q t} \\ &+ i \sum_{q, \text{nn}} \lambda_q [\hat{\sigma}^+(t) \hat{\sigma}_{\text{nn}}^-(t) \hat{b}_{q, \text{nn}}(0) e^{-i\omega_q t} + \text{H.c.}], \end{aligned} \quad (\text{A10a})$$

$$\hat{\xi}_b^{aa}(t) = i \sum_q \lambda_q \hat{C}(t) [\hat{\sigma}^-(t) \hat{b}_q(0) e^{-i\omega_q t} - \text{H.c.}], \quad (\text{A10b})$$

$$\begin{aligned} \hat{\xi}_c^+(t) &= -i \sum_q \lambda_q \hat{C}(t) \hat{c}_q^\dagger(0) \hat{\sigma}^z(t) e^{i\omega_q t} \\ &+ i \sum_{q, \text{nn}} \lambda_q [\hat{\sigma}^+(t) \hat{\sigma}_{\text{nn}}^+(t) \hat{c}_{q, \text{nn}}(0) e^{-i\omega_q t} + \text{H.c.}], \end{aligned} \quad (\text{A10c})$$

$$\hat{\xi}_c^{aa}(t) = i \sum_q \lambda_q \hat{C}(t) [\hat{c}_q^\dagger(0) \hat{\sigma}^-(t) e^{i\omega_q t} - \text{H.c.}]. \quad (\text{A10d})$$

One can compute the noise covariance in the Born-Markov approximation $2\pi D(0)[\lambda^{b/c}(0)]^2 = \kappa/2$, of which the nonvanishing ones read

$$\langle \hat{\xi}_b^+(t) \hat{\xi}_b^-(t') \rangle = \frac{\kappa}{2} [\hat{C}(t) \hat{\sigma}^{ii}(t) + \hat{N}(t) \hat{\sigma}^{aa}(t)] \delta(t - t'), \quad (\text{A11a})$$

$$\langle \hat{\xi}_b^-(t) \hat{\xi}_b^+(t') \rangle = \frac{\kappa}{2} [\hat{N}(t) - \hat{C}(t)] \hat{\sigma}^{aa}(t) \delta(t - t'), \quad (\text{A11b})$$

$$\langle \hat{\xi}_b^+(t) \hat{\xi}_b^{aa}(t') \rangle = -\frac{\kappa}{2} \hat{C}(t) \hat{\sigma}^+(t) \delta(t - t'), \quad (\text{A11c})$$

$$\langle \hat{\xi}_b^{aa}(t) \hat{\xi}_b^-(t') \rangle = -\frac{\kappa}{2} \hat{C}(t) \hat{\sigma}^-(t) \delta(t - t'), \quad (\text{A11d})$$

$$\langle \hat{\xi}_b^{aa}(t) \hat{\xi}_b^{aa}(t') \rangle = \frac{\kappa}{2} \hat{C}(t) \hat{\sigma}^{ii}(t) \delta(t - t'), \quad (\text{A11e})$$

for facilitated activation, and

$$\langle \hat{\xi}_c^+(t) \hat{\xi}_c^-(t') \rangle = \frac{\kappa}{2} \hat{C}(t) \hat{\sigma}^{aa}(t) \delta(t - t'), \quad (\text{A12a})$$

$$\langle \hat{\xi}_c^-(t) \hat{\xi}_c^+(t') \rangle = \frac{\kappa}{2} \hat{C}(t) [\hat{\sigma}^{aa}(t) + \hat{n}(t)] \delta(t - t'),$$

$$\langle \hat{\xi}_c^-(t) \hat{\xi}_c^{aa}(t') \rangle = \frac{\kappa}{2} \hat{C}(t) \hat{\sigma}^-(t) \delta(t - t'), \quad (\text{A12b})$$

$$\langle \hat{\xi}_c^{aa}(t) \hat{\xi}_c^+(t') \rangle = \frac{\kappa}{2} \hat{C}(t) \hat{\sigma}^+(t) \delta(t - t'), \quad (\text{A12c})$$

$$\langle \hat{\xi}_c^{aa}(t) \hat{\xi}_c^{aa}(t') \rangle = \frac{\kappa}{2} \hat{C}(t) \hat{\sigma}^{aa}(t) \delta(t - t'), \quad (\text{A12d})$$

for the inverse process.

Then the covariance of the noise operators $\hat{\xi}_f^{x/y/aa}$ arising from the above two processes can be obtained through the combinations according to

$$\hat{\xi}_f^{+/aa} = \hat{\xi}_b^{+/aa} + \hat{\xi}_c^{+/aa}, \quad (\text{A13a})$$

$$\hat{\xi}_f^x = \hat{\xi}_f^+ + \hat{\xi}_f^-, \quad (\text{A13b})$$

$$\hat{\xi}_f^y = -i\hat{\xi}_f^+ + i\hat{\xi}_f^-. \quad (\text{A13c})$$

Then the nonvanishing covariance is

$$\langle \hat{\xi}_f^x(t) \hat{\xi}_f^x(t') \rangle = \kappa [\hat{C}(t) \hat{n}(t) + \hat{N}(t) \hat{\sigma}^{aa}(t)] \delta(t - t'), \quad (\text{A14a})$$

$$\langle \hat{\xi}_f^y(t) \hat{\xi}_f^y(t') \rangle = \kappa [\hat{C}(t) \hat{n}(t) + \hat{N}(t) \hat{\sigma}^{aa}(t)] \delta(t - t'), \quad (\text{A14b})$$

$$\langle \hat{\xi}_f^{aa}(t) \hat{\xi}_f^{aa}(t') \rangle = \frac{\kappa}{2} \hat{C}(t) \hat{n}(t) \delta(t - t'), \quad (\text{A14c})$$

$$\langle \hat{\xi}_f^{aa}(t) \hat{\xi}_f^x(t') \rangle = i \frac{\kappa}{2} \hat{C}(t) \hat{\sigma}^y(t) \delta(t - t'), \quad (\text{A14d})$$

$$\langle \hat{\xi}_f^{aa}(t) \hat{\xi}_f^y(t') \rangle = -i \frac{\kappa}{2} \hat{C}(t) \hat{\sigma}^x(t) \delta(t - t'). \quad (\text{A14e})$$

The overall noise covariance is obtained via summing up those generated from the above three processes (i.e., spontaneous decay and incoherent contact activation/inactivation), yielding the correlator (4) in the main text.

APPENDIX B: PERTURBATIVE INTEGRATION OF COHERENCE FIELD

Our task is to evaluate

$$\mathcal{Z} = \int \mathcal{D}[\sigma^x, \tilde{\sigma}^x, \sigma^y, \tilde{\sigma}^y] e^{-S_\sigma - S_{\rho, \sigma}}, \quad (\text{B1})$$

with the action $S_{\rho, \sigma}$ given by Eq. (12) and

$$S_\sigma = - \int \left[\tilde{\sigma}^x \left(\mathcal{F}_{\sigma^x} + \frac{M_{xx}}{2} \tilde{\sigma}^x \right) + \tilde{\sigma}^y \left(\mathcal{F}_{\sigma^y} + \frac{M_{yy}}{2} \tilde{\sigma}^y \right) \right], \quad (\text{B2})$$

in which

$$\mathcal{F}_{\sigma^x} = -\frac{n\kappa + \gamma}{2} \sigma^x - \kappa \sigma^x \rho - \Omega \sigma^y \sigma^x, \quad (\text{B3a})$$

$$\mathcal{F}_{\sigma^y} = -\frac{n\kappa + \gamma}{2} \sigma^y + \Omega (\sigma^x)^2 + [2\Omega(n - 2\rho) - \kappa \sigma^y] \rho. \quad (\text{B3b})$$

We decompose the action $S_\sigma = S_{\sigma,0} + S_{\sigma,\text{int}}$, in which the former represents the respective relaxation of the $\sigma^{x/y}$ with

$$S_{\sigma,0} = \int \tilde{\sigma}^x \left(\frac{n\kappa + \gamma}{2} \sigma^x - \frac{n}{2} \tilde{\sigma}^x \right) + \int \tilde{\sigma}^y \left(\frac{n\kappa + \gamma}{2} \sigma^y - \frac{n}{2} \tilde{\sigma}^y \right), \quad (\text{B4})$$

and the latter represents interactions between them.

The coarse-grained action $\langle S_{\rho,\sigma} \rangle$ follows from

$$\langle S_{\rho,\sigma} \rangle = -\ln \left(\frac{\int \prod_{i=x,y} \mathcal{D}[\sigma^i, \tilde{\sigma}^i] e^{-S_{\rho,\sigma} - S_\sigma}}{\int \prod_{i=x,y} \mathcal{D}[\sigma^i, \tilde{\sigma}^i] e^{-S_{\sigma,0}}} \right). \quad (\text{B5})$$

$$\langle S \rangle_{X_0} = \int \left\{ \left[\frac{n\kappa + \gamma}{2} + \frac{16\Omega^2 n}{(\kappa n + \gamma)^3} + \kappa \rho \right] \tilde{\sigma}^y \sigma^y - \frac{1 + 2\kappa \rho}{2} n (\tilde{\sigma}^y)^2 - \frac{2\Omega^2 (\sigma^y)^2}{(n\kappa + \gamma)^2} \right\} - \int \left[2\Omega \rho (n - 2\rho) + \frac{4\Omega n}{(\kappa n + \gamma)^2} \left(1 + 2\kappa \rho - \frac{4\kappa \rho}{n\kappa + \gamma} \right) \right] \tilde{\sigma}^y - \int \left[\Omega \tilde{\rho} \rho - \frac{2\Omega}{\kappa n + \gamma} \left(1 - \frac{2\kappa \rho}{n\kappa + \gamma} \right) \right] \sigma^y. \quad (\text{B7})$$

We proceed to compute the average of Eq. (B7) over the $\sigma^y, \tilde{\sigma}^y$ fields. This will lead to an action,

$$\langle S \rangle_{X_0, Y_0} = -\ln \left\langle e^{\int [-\frac{1}{2} \sigma^y Y_1 (\sigma^y)^T + \mathbf{b} (\sigma^y)^T]} \right\rangle_{X_0, Y_0}, \quad (\text{B8})$$

where the vectorial notation $\sigma^y = (\sigma^y \quad \tilde{\sigma}^y)$, and the matrices Y_0, Y_1 , and \mathbf{b} are given by

$$Y_0 = \begin{pmatrix} 0 & \frac{n\kappa + \gamma}{2} \\ \frac{n\kappa + \gamma}{2} & -n \end{pmatrix}, \quad (\text{B9a})$$

$$Y_1 = \begin{pmatrix} -\frac{4\Omega^2}{(n\kappa + \gamma)^2} & \kappa \rho + \frac{16\Omega^2 n}{(n\kappa + \gamma)^3} \\ \kappa \rho + \frac{16\Omega^2 n}{(n\kappa + \gamma)^3} & -2\kappa n \rho \end{pmatrix}, \quad (\text{B9b})$$

$$\mathbf{b}^T = \begin{pmatrix} \Omega \tilde{\rho} \rho - \frac{2\Omega}{n\kappa + \gamma} \left(1 - \frac{2\kappa \rho}{n\kappa + \gamma} \right) \\ 2\Omega \rho (n - 2\rho) + \frac{4n\Omega}{(n\kappa + \gamma)^2} \left(1 + 2\kappa \rho - \frac{4\kappa \rho}{n\kappa + \gamma} \right) \end{pmatrix} \quad (\text{B9c})$$

The leading and subleading order corrections S_1, S_2 arise from $\mathbf{b} Y_0^{-1} \mathbf{b}$ and $\mathbf{b} Y_0^{-1} Y_1 Y_0^{-1} \mathbf{b}$, where

$$S_1 = -\frac{2n\Omega^2 \rho^2 \tilde{\rho}^2}{(n\kappa + \gamma)^2} - \frac{4\Omega^2 \tilde{\rho}}{n\kappa + \gamma} (n\rho^2 - 2\rho^3) - \frac{16n\Omega^2 \kappa \tilde{\rho} \rho^2}{(n\kappa + \gamma)^3} \left(1 - \frac{1}{n\kappa + \gamma} \right), \quad (\text{B10a})$$

$$S_2 = -\frac{256n^2 \Omega^4 \tilde{\rho} \rho}{(n\kappa + \gamma)^7} + \frac{96n^2 \Omega^4 \tilde{\rho}^2 \rho^2}{(n\kappa + \gamma)^6} + \frac{8n\Omega^2 \kappa \tilde{\rho} \rho^3}{(n\kappa + \gamma)^2} + \frac{16n\Omega^2 \kappa \tilde{\rho} \rho^2}{(n\kappa + \gamma)^3} + \dots, \quad (\text{B10b})$$

where we retain the leading-order corrections to each coupling constant. The effective density field action in the main text is the sum of Eqs. (11), (B10a), and (B10b).

Before leaving this section, we provide the MF approach to eliminating $\sigma^{x/y}$ as a comparison. After adiabatically eliminating the coherence fields, the equation of motion for the

We start with integrating out $\sigma^x, \tilde{\sigma}^x$, via averaging $\exp[-\int \frac{1}{2} \sigma^x X_1 (\sigma^x)^T]$ over $\exp[-\int \frac{1}{2} \sigma^x X_0 (\sigma^x)^T]$, where the vectorial representation $\sigma^x = (\sigma^x \quad \tilde{\sigma}^x)$, and

$$X_0 = \begin{pmatrix} 0 & \frac{n\kappa + \gamma}{2} \\ \frac{n\kappa + \gamma}{2} & -n \end{pmatrix}, \quad (\text{B6a})$$

$$X_1 = \begin{pmatrix} -2\Omega \tilde{\sigma}^y & \kappa \rho + \Omega \sigma^y \\ \kappa \rho + \Omega \sigma^y & -2\kappa \rho n \end{pmatrix}. \quad (\text{B6b})$$

The action S now reduces to

active field with a conserved total density reads

$$\partial_t \rho = D_\rho \nabla^2 \rho + (\kappa n - 1) \rho + 2 \left(\frac{2\Omega^2 n}{n\kappa + \gamma} - \kappa \right) \rho^2 - \frac{8\Omega^2 \rho^3}{n\kappa + \gamma} + \xi^\rho. \quad (\text{B11})$$

Compare Eq. (B11) with the one associated with the effective action (13), the dynamic path integral approach provides us the important piece of information that in the quantum region, the additive noises of the coherence fields with a covariance increases with the total density and makes the system more susceptible to fluctuations near the absorbing phase at high total densities.

APPENDIX C: FUNCTIONAL RENORMALIZATION GROUP ANALYSIS

In this Appendix, we provide details of the nonperturbative renormalization group (NPRG) approach to discontinuous APTs based on the Wetterich equation [54],

$$\partial_k \Gamma_k = \frac{1}{2} \text{Tr} \left[(\Gamma_k^{(2)} + R_k)^{-1} \partial_k R_k \right]. \quad (\text{C1})$$

Here, in out-of-equilibrium settings, Γ_k is the nonequilibrium equivalent of the Gibbs free energy in the presence of a masslike regulator R_k [45,55], defined as the Legendre transform of the generating functional of connected functions $\mathcal{W}_k = \ln \mathcal{Z}_k[j, \tilde{j}]$, viz.,

$$\Gamma_k[\rho, \tilde{\rho}] = \int (j\rho + \tilde{j}\tilde{\rho}) - \mathcal{W}_k[j, \tilde{j}], \quad (\text{C2})$$

where the scale-dependent partition function \mathcal{Z}_k is built from adding a momentum-dependent term ΔS_k to the bare action S evaluated with a uniform field,

$$\mathcal{Z}_k[j, \tilde{j}] = \int \mathcal{D}[\rho, \tilde{\rho}] \exp \left[-S - \Delta S_k + \int (j\rho + \tilde{j}\tilde{\rho}) \right] \quad (\text{C3})$$

and

$$\Delta S_k = \frac{1}{2} \int \boldsymbol{\rho}^T \mathbf{R}_k \boldsymbol{\rho}, \quad (\text{C4})$$

where $\boldsymbol{\rho}^T = (\rho \quad \tilde{\rho})$, and \mathbf{R}_k is a 2×2 matrix of quadratic functions, where the cutoff momentum k varies within the range $k \in [0, \Lambda]$.

We apply the local potential approximation (LPA) ansatz [55], according to which the bare interaction part of the action Γ_k is evaluated with a uniform background field,

$$V^{-1} \ln \Gamma_{0,k} = U_k(\delta_j \ln \mathcal{Z}_{0,k}|_{j,\tilde{j}}, \delta_{\tilde{j}} \ln \mathcal{Z}_{0,k}|_{j,\tilde{j}}), \quad (\text{C5})$$

where V is the space volume and the running local action (analogous to the local potential in the equilibrium cases) $U_k(\rho, \tilde{\rho})$ is given by

$$U_k = \tilde{\rho}[u_{2,k}\rho + u_{3,k}\rho^2 + u_{4,k}\rho^3] - \mu_{1,k}\tilde{\rho}\rho - \mu_{2,k}\tilde{\rho}\rho^2. \quad (\text{C6})$$

The two (running) noiseless saddle-point solutions $\{\tilde{\rho} = 0, \rho = \alpha_k\}$ and $\{\tilde{\rho} = 0, \rho = 0\}$ to the action U_k correspond to the densities of the absorbing and active phases, respectively, which are also the running local minima of the effective

potential,

$$\Phi_k(\rho) = \frac{u_{2,k}}{2}\rho^2 + \frac{u_{3,k}}{3}\rho^3 + \frac{u_{4,k}}{4}\rho^4. \quad (\text{C7})$$

With a convenient choice of the θ regulator [55],

$$\mathbf{R}_k(q) = \begin{pmatrix} 0 & R_k(q) \\ R_k(q) & 0 \end{pmatrix}, \quad (\text{C8})$$

where $R_k(q) = k^2(1 - q^2/k^2)\theta(1 - q^2/k^2)$, the flow equation for the dimensionless potential $U \rightarrow k^{-(d+2)}U$ in terms of the dimensionless fields $\rho \rightarrow k^{-d}\rho$, $\tilde{\rho} \rightarrow \tilde{\rho}$ and the RG time $s = \ln(k/\Lambda)$ with vanishing anomalous dimension follows from integrating over frequencies and momenta,

$$\partial_s U = -(d+2)U + d\rho U^{(1,0)} + \frac{V_d}{\sqrt{1 - \frac{U^{(2,0)}U^{(0,2)}}{(U^{(1,1)}+1)^2}}}, \quad (\text{C9})$$

where $V_d = [2^{d-1}d\pi^{d/2}\Gamma(d/2)]^{-1}$ and we have introduced the notation $U^{(n,m)} = \partial_{\rho}^n \partial_{\tilde{\rho}}^m U$ and scaled away the k -independent diffusivity D_{ρ} . Hereafter, we omit the explicit dependence on s of the running parameters.

We evaluate the flow equation (C9) at the running uniform, noiseless saddle-point solution with finite active densities and arrive at

$$\partial_s u_2 = -2u_2 - \frac{V_d(c_2 - \alpha c_3)\mu_1}{(1+c_1)^2} - \frac{V_d c_2 \alpha [\mu_1 c_2 - 3c_3 \alpha (\mu_1 + \alpha \mu_2)]}{(1+c_1)^3} + \mathcal{O}[(1+c_1)^{-4}], \quad (\text{C10a})$$

$$\partial_s u_3 = -(2-d)u_3 - \frac{V_d [c_3(\mu_1 - \alpha \mu_2) + c_2 \mu_2]}{(1+c_1)^2} + \frac{2V_d c_2 [\mu_1(c_2 - 6\alpha c_3) - \alpha c_2 \mu_2]}{(1+c_1)^3} + \mathcal{O}[(1+c_1)^{-4}], \quad (\text{C10b})$$

$$\partial_s u_4 = -2(1-d)u_4 - \frac{V_d c_3 \mu_2}{(1+c_1)^2} + \frac{V_d \{c_3^2 \alpha (\mu_1 + \alpha \mu_2) + c_2 [3c_3(\mu_1 + 2\alpha \mu_2) + 2c_2 \mu_2]\}}{(1+c_1)^3} + \mathcal{O}[(1+c_1)^{-4}], \quad (\text{C10c})$$

$$\partial_s \mu_1 = -2\mu_1 - \frac{2V_d \mu_1 \mu_2}{(1+c_1)^2} - \frac{4V_d \{\alpha \mu_1 \mu_2 (c_2 + 10\alpha c_3) + [\alpha^2 \mu_2^2 (9c_2 + 11\alpha c_3) + \mu_1^2 (\alpha c_3 - c_2)]\}}{(1+c_1)^3} + \mathcal{O}[(1+c_1)^{-4}], \quad (\text{C10d})$$

$$\partial_s \mu_2 = -(2-d)\mu_2 - \frac{2V_d \mu_2^2}{(1+c_1)^2} + \frac{2V_d [8c_2 \mu_2 (\mu_1 + 2\alpha \mu_2) + c_3 (2\mu_1^2 + 13\alpha \mu_1 \mu_2 + 13\alpha^2 \mu_2^2)]}{(1+c_1)^3} + \mathcal{O}[(1+c_1)^{-4}], \quad (\text{C10e})$$

where α is the running minimum related to the active phase, and we have introduced $c_1 = u_2 + 2u_3\alpha + 3u_4\alpha^2$, $c_2 = 2u_3 + 6u_4\alpha$, and $c_3 = 6u_4$ to obtain a friendlier expression.

Starting with the MF values as the initial conditions, we numerically integrate the flow equations until either the two minima become degenerate or the values of the dimensional counterparts of the running coefficients no longer evolve with decreasing s . Plugging the renormalized coefficients into (C7) and determining the phases accordingly yield the results shown in the main text.

APPENDIX D: NUMERICAL INTEGRATION SCHEME

Numerical integration of the Langevin equations with multiplicative noise is performed by an operator-splitting scheme [56,57], which consists in integrating the stochastic part first, by sampling the time-dependent solution of the corresponding Fokker-Planck equation (FPE), and then using the generated value to evolve the deterministic part of the equation by any standard numerical integration method.

The Langevin equation for the active density field reads

$$\partial_t \rho = \alpha + \beta \rho + f(\rho) + \sigma \sqrt{\rho} \xi, \quad (\text{D1})$$

where

$$\alpha = \tau n + \frac{D_{\rho}}{(dx)^2} \sum_{i=1}^{2d} \rho(\mathbf{r} + \mathbf{e}_i, t), \quad (\text{D2})$$

arising from discretizing the Laplacian $\nabla^2 \rho$ of site \mathbf{r}_i on a d -dimensional square lattice of mesh size dx , and

$$\beta = -u_2 - 2d \frac{D_{\rho}}{(dx)^2}, \quad (\text{D3a})$$

$$f(\rho) = -u_3 \rho^2 - u_4 \rho^3, \quad (\text{D3b})$$

$$\sigma^2 = 1 + \kappa n + \frac{4\Omega^2 n \rho}{(n\kappa + \gamma)^2}. \quad (\text{D3c})$$

The stochastic value ρ^* is generated according to the conditional transition probability density function $P(\rho, t) =$

$P(\rho(t) = \rho | \rho(0) = \rho_0)$, which reads

$$P(\rho, t) = \lambda e^{-\lambda(\rho_0 e^{\beta t} + \rho)} \left[\frac{\rho}{\rho_0 e^{\beta t}} \right]^{\mu/2} I_{\mu} \left(2\lambda \sqrt{\rho_0 \rho e^{\beta t}} \right), \quad (\text{D4})$$

where I_{μ} is a Bessel function of the order of μ , and

$$\lambda = \frac{2\beta}{\sigma^2(e^{\beta t} - 1)}, \quad \mu = -1 + \frac{2\alpha}{\sigma^2}. \quad (\text{D5})$$

Using the Taylor-series expansion of the Bessel function, we can sample the value ρ^* according to the following

mixture:

$$\rho^* \sim \text{Gamma}[\mu + 1 + \text{Poisson}[\lambda \rho_0 e^{\beta t}]] / \lambda, \quad (\text{D6})$$

and then we use ρ^* as the initial condition for the remaining part of the equation,

$$\rho(\mathbf{r}, t + dt) = \rho^* + f(\rho^*)dt. \quad (\text{D7})$$

The equation for the total density is integrated via the Euler's method. For the simulations, we fix $\gamma=2$, $D_T=D_n=1$, $\tau = 10^{-7}$, $b = 0.01$.

-
- [1] F. Wilczek, Quantum time crystals, *Phys. Rev. Lett.* **109**, 160401 (2012).
- [2] A. Shapere and F. Wilczek, Classical time crystals, *Phys. Rev. Lett.* **109**, 160402 (2012).
- [3] P. Bruno, Impossibility of spontaneously rotating time crystals: A no-go theorem, *Phys. Rev. Lett.* **111**, 070402 (2013).
- [4] H. Watanabe and M. Oshikawa, Absence of quantum time crystals, *Phys. Rev. Lett.* **114**, 251603 (2015).
- [5] V. Khemani, A. Lazarides, R. Moessner, and S. L. Sondhi, Phase structure of driven quantum systems, *Phys. Rev. Lett.* **116**, 250401 (2016).
- [6] N. Y. Yao, A. C. Potter, I.-D. Potirniche, and A. Vishwanath, Discrete time crystals: Rigidity, criticality, and realizations, *Phys. Rev. Lett.* **118**, 030401 (2017).
- [7] S. Choi, J. Choi, R. Landig, G. Kucsko, H. Zhou, J. Isoya, F. Jelezko, S. Onoda, H. Sumiya, V. Khemani, C. von Keyserlingk, N. Y. Yao, E. Demler, and M. D. Lukin, Observation of discrete time-crystalline order in a disordered dipolar many-body system, *Nature (London)* **543**, 221 (2017).
- [8] J. Smits, L. Liao, H. T. C. Stoof, and P. van der Straten, Observation of a space-time crystal in a superfluid quantum gas, *Phys. Rev. Lett.* **121**, 185301 (2018).
- [9] F. M. Gambetta, F. Carollo, M. Marcuzzi, J. P. Garrahan, and I. Lesanovsky, Discrete time crystals in the absence of manifest symmetries or disorder in open quantum systems, *Phys. Rev. Lett.* **122**, 015701 (2019).
- [10] D. Bluvstein, A. Omran, H. Levine, A. Keesling, G. Semeghini, S. Ebadi, T. T. Wang, A. A. Michailidis, N. Maskara, W. W. Ho, S. Choi, M. Serbyn, M. Greiner, V. Vuletić, and M. D. Lukin, Controlling quantum many-body dynamics in driven Rydberg atom arrays, *Science* **371**, 1355 (2021).
- [11] H. Keßler, P. Kongkhambut, C. Georges, L. Mathey, J. G. Cosme, and A. Hemmerich, Observation of a dissipative time crystal, *Phys. Rev. Lett.* **127**, 043602 (2021).
- [12] S. Sarkar and Y. Dubi, Signatures of discrete time-crystallinity in transport through an open fermionic chain, *Commun. Phys.* **5**, 155 (2022).
- [13] F. Piazza and H. Ritsch, Self-ordered limit cycles, chaos, and phase slippage with a superfluid inside an optical resonator, *Phys. Rev. Lett.* **115**, 163601 (2015).
- [14] C.-K. Chan, T. E. Lee, and S. Gopalakrishnan, Limit-cycle phase in driven-dissipative spin systems, *Phys. Rev. A* **91**, 051601(R) (2015).
- [15] F. Iemini, A. Russomanno, J. Keeling, M. Schirò, M. Dalmonte, and R. Fazio, Boundary time crystals, *Phys. Rev. Lett.* **121**, 035301 (2018).
- [16] B. Buča, J. Tindall, and D. Jaksch, Non-stationary coherent quantum many-body dynamics through dissipation, *Nat. Commun.* **10**, 1 (2019).
- [17] X. Nie and W. Zheng, Mode softening in time-crystalline transitions of open quantum systems, *Phys. Rev. A* **107**, 033311 (2023).
- [18] Y. H. Chen and X. Zhang, Realization of an inherent time crystal in a dissipative many-body system, *Nat. Commun.* **14**, 6161 (2023).
- [19] M. Krishna, P. Solanki, M. Hajdušek, and S. Vinjanampathy, Measurement-induced continuous time crystals, *Phys. Rev. Lett.* **130**, 150401 (2023).
- [20] C. Lledó and M. H. Szymańska, A dissipative time crystal with or without Z_2 symmetry breaking, *New J. Phys.* **22**, 075002 (2020).
- [21] J. Sheng, X. Wei, C. Yang, and H. Wu, Self-organized synchronization of phonon lasers, *Phys. Rev. Lett.* **124**, 053604 (2020).
- [22] D. Ding, Z. Bai, Z. Liu, B. Shi, G. Guo, W. Li, and C. S. Adams, Ergodicity breaking from Rydberg clusters in a driven-dissipative many-body system, *Sci. Adv.* **10**, ead15893 (2024).
- [23] X. Wu, Z. Wang, F. Yang, R. Gao, C. Liang, M. K. Tey, X. Li, T. Pohl, and L. You, Dissipative time crystal in a strongly interacting Rydberg gas, *Nat. Phys.* (2024), doi:10.1038/s41567-024-02542-9.
- [24] K. Wadenpfehl and C. S. Adams, Emergence of synchronization in a driven-dissipative hot Rydberg vapor, *Phys. Rev. Lett.* **131**, 143002 (2023).
- [25] H. Keßler, J. G. Cosme, M. Hemmerling, L. Mathey, and A. Hemmerich, Emergent limit cycles and time crystal dynamics in an atom-cavity system, *Phys. Rev. A* **99**, 053605 (2019).
- [26] P. Kongkhambut, J. Skulte, L. Mathey, J. G. Cosme, A. Hemmerich, and H. Keßler, Observation of a continuous time crystal, *Science* **377**, 670 (2022).
- [27] C. Tang and P. Bak, Mean field-theory of self-organized critical phenomena, *J. Stat. Phys.* **51**, 797 (1988).
- [28] D. Sornette, Critical phase transitions made self-organized: A dynamical system feedback mechanism for self-organized criticality, *J. Phys. I France* **2**, 2065 (1992).
- [29] M. Paczuski, S. Maslov, and P. Bak, Field theory for a model of self-organized criticality, *Europhys. Lett.* **27**, 97 (1994).

- [30] G. Grinstein, Generic scale invariance and self-organized criticality, in *Scale Invariance, Interfaces, and Non-Equilibrium Dynamics*, edited by A. McKane, M. Droz, J. Vannimenus, and D. Wolf (Springer US, Boston, MA, 1995), pp. 261–293.
- [31] L. Gil and D. Sornette, Landau-Ginzburg theory of self-organized criticality, *Phys. Rev. Lett.* **76**, 3991 (1996).
- [32] R. Dickman, A. Vespignani, and S. Zapperi, Self-organized criticality as an absorbing-state phase transition, *Phys. Rev. E* **57**, 5095 (1998).
- [33] R. Dickman, M. A. Muñoz, A. Vespignani, and S. Zapperi, Paths to self-organized criticality, *Braz. J. Phys.* **30**, 27 (2000).
- [34] V. Buendía, S. di Santo, J. A. Bonachela, and M. A. Muñoz, Feedback mechanisms for self-organization to the edge of a phase transition, *Front. Phys.* **8**, 333 (2020).
- [35] S. di Santo, R. Burioni, A. Vezzani, and M. A. Muñoz, Self-organized bistability associated with first-order phase transitions, *Phys. Rev. Lett.* **116**, 240601 (2016).
- [36] M. Marcuzzi, M. Buchhold, S. Diehl, and I. Lesanovsky, Absorbing state phase transition with competing quantum and classical fluctuations, *Phys. Rev. Lett.* **116**, 245701 (2016).
- [37] D.-S. Ding, H. Busche, B.-S. Shi, G.-C. Guo, and C. S. Adams, Phase diagram and self-organizing dynamics in a thermal ensemble of strongly interacting Rydberg atoms, *Phys. Rev. X* **10**, 021023 (2020).
- [38] S. Helmrich, A. Arias, G. Lochead, T. M. Wintermantel, M. Buchhold, S. Diehl, and S. Whitlock, Signatures of self-organized criticality in an ultracold atomic gas, *Nature (London)* **577**, 481 (2020).
- [39] C. Gardiner and P. Zoller, *Quantum Noise: A Handbook of Markovian and non-Markovian Quantum Stochastic Methods with Applications to Quantum Optics* (Springer Science & Business Media, Berlin, Germany, 2004).
- [40] L. Pan, X. Chen, Y. Chen, and H. Zhai, Non-Hermitian linear response theory, *Nat. Phys.* **16**, 767 (2020).
- [41] M. Buchhold, B. Everest, M. Marcuzzi, I. Lesanovsky, and S. Diehl, Nonequilibrium effective field theory for absorbing state phase transitions in driven open quantum spin systems, *Phys. Rev. B* **95**, 014308 (2017).
- [42] H.-K. Janssen, On a Lagrangean for classical field dynamics and renormalization group calculations of dynamical critical properties, *Z. Phys. B* **23**, 377 (1976).
- [43] P. C. Martin, E. D. Siggia, and H. A. Rose, Statistical dynamics of classical systems, *Phys. Rev. A* **8**, 423 (1973).
- [44] M. F. Wehner and W. G. Wolfer, Numerical evaluation of path-integral solutions to Fokker-Planck equations, *Phys. Rev. A* **27**, 2663 (1983).
- [45] L. Canet, H. Chaté, and B. Delamotte, General framework of the non-perturbative renormalization group for non-equilibrium steady states, *J. Phys. A: Math. Theor.* **44**, 495001 (2011).
- [46] U. C. Täuber, *Critical Dynamics: A Field Theory Approach to Equilibrium and Non-Equilibrium Scaling Behavior* (Cambridge University Press, Cambridge, United Kingdom, 2014).
- [47] K. Klocke and M. Buchhold, Controlling excitation avalanches in driven Rydberg gases, *Phys. Rev. A* **99**, 053616 (2019).
- [48] M. C. Cross and P. C. Hohenberg, Pattern formation outside of equilibrium, *Rev. Mod. Phys.* **65**, 851 (1993).
- [49] O. Scarlatella, R. Fazio, and M. Schiró, Emergent finite frequency criticality of driven-dissipative correlated lattice bosons, *Phys. Rev. B* **99**, 064511 (2019).
- [50] T. E. Lee, H. Häffner, and M. C. Cross, Antiferromagnetic phase transition in a nonequilibrium lattice of Rydberg atoms, *Phys. Rev. A* **84**, 031402(R) (2011).
- [51] Z.-K. Liu, K.-H. Sun, A. Cabot, F. Carollo, J. Zhang, Z.-Y. Zhang, L.-H. Zhang, B. Liu, T.-Y. Han, Q. Li *et al.*, Microwave control of collective quantum jump statistics of a dissipative Rydberg gas, [arXiv:2402.04815](https://arxiv.org/abs/2402.04815).
- [52] T. E. Lee, H. Häffner, and M. C. Cross, Collective quantum jumps of Rydberg atoms, *Phys. Rev. Lett.* **108**, 023602 (2012).
- [53] H. Li, K. Sun, and W. Yi, Collective quantum stochastic resonance in Rydberg atoms, [arXiv:2401.16894](https://arxiv.org/abs/2401.16894).
- [54] C. Wetterich, Exact evolution equation for the effective potential, *Phys. Lett. B* **301**, 90 (1993).
- [55] N. Dupuis, L. Canet, A. Eichhorn, W. Metzner, J. Pawłowski, M. Tissier, and N. Wschebor, The nonperturbative functional renormalization group and its applications, *Phys. Rep.* **910**, 1 (2021).
- [56] L. Pechenik and H. Levine, Interfacial velocity corrections due to multiplicative noise, *Phys. Rev. E* **59**, 3893 (1999).
- [57] I. Dornic, H. Chaté, and M. A. Muñoz, Integration of Langevin equations with multiplicative noise and the viability of field theories for absorbing phase transitions, *Phys. Rev. Lett.* **94**, 100601 (2005).
- [58] R. Gernert, C. Emary, and S. H. L. Klapp, Waiting time distribution for continuous stochastic systems, *Phys. Rev. E* **90**, 062115 (2014).
- [59] N. V. Kampen, *Stochastic Processes in Physics and Chemistry*, 3rd ed., North-Holland personal library (Elsevier, Singapore, 2007).
- [60] R. P. Boland, T. Galla, and A. J. McKane, How limit cycles and quasi-cycles are related in systems with intrinsic noise, *J. Stat. Mech.* (2008) P09001.
- [61] A. Cabot, L. S. Muhle, F. Carollo, and I. Lesanovsky, Quantum trajectories of dissipative time crystals, *Phys. Rev. A* **108**, L041303 (2023).
- [62] P. Grassberger, Critical behaviour of the Drossel-Schwabl forest fire model, *New J. Phys.* **4**, 17 (2002).
- [63] O. Kinouchi, L. Brochini, A. A. Costa, J. G. F. Campos, and M. Copelli, Stochastic oscillations and dragon king avalanches in self-organized quasi-critical systems, *Sci. Rep.* **9**, 3874 (2019).
- [64] I. R. Epstein and K. Showalter, Nonlinear chemical dynamics: Oscillations, patterns, and chaos, *J. Phys. Chem.* **100**, 13132 (1996).
- [65] R. Lefever and G. Nicolis, Chemical instabilities and sustained oscillations, *J. Theor. Biol.* **30**, 267 (1971).
- [66] M. Doi, Stochastic theory of diffusion-controlled reaction, *J. Phys. A: Math. Gen.* **9**, 1479 (1976).
- [67] L. Peliti, Path integral approach to birth-death processes on a lattice, *J. Phys. France* **46**, 1469 (1985).
- [68] K. J. Wiese, Coherent-state path integral versus coarse-grained effective stochastic equation of motion: From reaction diffusion to stochastic sandpiles, *Phys. Rev. E* **93**, 042117 (2016).

- [69] B. D. Malamud, G. Morein, and D. L. Turcotte, Forest fires: An example of self-organized critical behavior, *Science* **281**, 1840 (1998).
- [70] N. Yoshioka, A sandpile experiment and its implications for self-organized criticality and characteristic earthquake, *Earth Planet. Space* **55**, 283 (2003).
- [71] J. M. Beggs and D. Plenz, Neuronal avalanches in neocortical circuits, *J. Neurosci.* **23**, 11167 (2003).
- [72] J. A. Bonachela and M. A. Muñoz, Self-organization without conservation: True or just apparent scale-invariance? *J. Stat. Mech.* (2009) P09009.
- [73] L. M. Sieberer, M. Buchhold, and S. Diehl, Keldysh field theory for driven open quantum systems, *Rep. Prog. Phys.* **79**, 096001 (2016).
- [74] A. Kamenev, *Field Theory of Non-equilibrium Systems*, 2nd ed. (Cambridge University Press, Cambridge, United Kingdom, 2023).